ACS OMEGA

Open Access

http://pubs.acs.org/journal/acsodf

Article

Xuanfei Baidu Decoction Alleviated Sepsis-Induced ALI by Modulating Gut Microbial Homeostasis and Promoting Inflammation Resolution: Bioinformatics and Experimental Study

Lei Yang, Sijia Zhang, Lingzhi Cui, Junxia Zhang, Shukun Zhang, Lanqiu Zhang, Lihua Cui, Caixia Li, Yuzhen Zhuo,* Yuhong Li,* and Ximo Wang*

Cite This: *ACS Omega* 2025, 10, 13105−13121

Read Online

ACCESS | Metrics & More | Article Recommendations

ABSTRACT: The Xuanfei Baidu Decoction (XFBD) has shown effective therapeutic potential for acute lung injury (ALI) induced by lipopolysaccharide and immunoglobin G immune complexes. Herein, the protective effects and mechanisms of XFBD were investigated in a sepsis-induced ALI mouse model along with its effects on gut microbiota. Notably, bioinformatics and molecular docking analyses revealed that XFBD components exhibited a strong binding affinity to G-protein-coupled receptor 18 (GPR18). In the murine ALI model—induced by cecal ligation and puncture (CLP)—XFBD markedly improved lung histopathology, reduced M1 macrophage polarization, and decreased pro-inflammatory cytokine levels in both lung tissues and MH-S macrophages. Furthermore, XFBD downregulated key inflammatory pathways, including nuclear factor (NF)-κB, phosphorylated-NF-κB, CCAAT/enhancer binding protein-δ, and the nucleotide-binding oligomerization domain-like receptor pyrin domain-containing 3/Caspase-1/gasdermin D axis. Additionally, XFBD restored the CLP-induced disruption in gut microbiota balance, increasing the abundance of Prevotellaceae and Ruminococcaceae_UCG_014. Altogether, the findings of this study suggest that XFBD alleviates CLP-induced ALI by modulating gut microbial homeostasis and inhibiting associated inflammatory pathways, particularly via GPR18 activation, presenting the promising therapeutic potential of XFBD for treating sepsis-induced ALI.

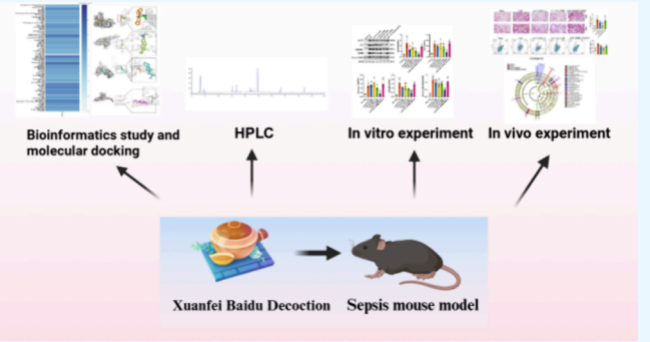

INTRODUCTION

Both acute lung injury (ALI) and acute respiratory distress syndrome (ARDS), a severe manifestation of ALI, are debilitating conditions, with pervasive inflammation, impaired gas exchange, and respiratory failure being characteristic symptoms. Various conditions, including pneumonia, sepsis, trauma, and aspiration, may lead to the development of these symptoms, contributing to increased rates of morbidity and mortality globally.[1] For instance, the incidence of sepsis-induced ALI/ARDS can reach up to 25−50%. A meta-analysis encompassing 72 clinical studies on ARDS from 1994 to 2006 and comprising 11,426 patients with ALI/ARDS reported a global mortality rate of 43%.[2] Reportedly, an excessive inflammatory response is a major characteristic symptom of ALI/ARDS, and it has led to controversies regarding the effectiveness of corticosteroids in improving mortality rates. For instance, late-stage administration of glucocorticoids for ARDS management has been associated with increased mortality.[3] ALI/ARDS imposes a substantial economic burden on families and societies, necessitating the search for specific therapies to be a major research focus.

Although increased vascular permeability, neutrophil infiltration, and an exaggerated inflammatory response have been identified as the primary causes of lung injury,[4] the molecular mechanisms underlying sepsis-induced ALI/ARDS remain elusive. Reportedly, resolvin D2 (RvD2) has been shown to facilitate the resolution of inflammation and promote tissue repair via the G-protein-coupled receptor 18 (GPR18) axis. The RvD2−GPR18 interaction selectively activates GPR18, which is present in both human- and murine-derived macrophages.[5] The RvD2−GPR18 signaling axis upregulates phagocytosis, modulates the expression of adhesion receptors, and influences cytokine production within phagocytes, ultimately promoting tissue repair and regeneration. Moreover,

Received: November 20, 2024
Revised: March 14, 2025
Accepted: March 20, 2025
Published: March 26, 2025

this RvD2−GPR18 axis does not compromise host defense but instead enhances host immunity in the presence of polymicrobial sepsis and bacterial infections, demonstrating its role in inflammation management and supporting tissue health.[6] Previously, a notable correlation has been reported for RvD2 and GPR18 expression on neutrophils in the peripheral blood of patients with sepsis and their clinical outcomes.[7] Furthermore, RvD1 can activate silent information regulator sirtuin 1 to regulate macrophage polarization, alleviating sepsis-induced ALI.[8] Additionally, we have previously reported that verbenalin can mitigate lipopolysaccharide (LPS)-induced ALI by activating the RvD2 receptor, GPR18.[9]

The severe acute respiratory syndrome coronavirus 2, the causative agent of Coronavirus Disease 2019 (COVID-19), has affected over 10 million individuals, underscoring the severity of this worldwide health crisis.[10] In China, traditional Chinese medicine (TCM) has shown efficacy in treating COVID-19.[11] According to the State Council of the People's Republic of China (2020), over 74,000 patients were treated with TCM, and an overall efficacy rate of >90% was achieved. The National Administration of TCM recommended "three medicines and three prescriptions" for clinical treatment of COVID-19. The "three medicines" include Jinhua Qinggan Granule, Lianhua Qingwen Capsule, and Xuebijing Injection, and the "three prescriptions" include Qingfei Paidu Decoction, Huashi Baidu Formula, and Xuanfei Baidu Granule. Additionally, the seventh edition of the "Diagnosis and Treatment Protocol for Novel Coronavirus Pneumonia" in China recommended Xuanfei Baidu Decoction (XFBD) as one of the three TCM remedies for common COVID-19 cases, showing promising clinical outcomes.[12] Reportedly, this intervention, using traditional Chinese medicine (TCM) known for its lung-ventilating and detoxifying properties, has shown promising results in treating COVID-19 by improving pulmonary injury, down-regulating proinflammatory cytokines, and reducing macrophage and neutrophil infiltration in LPS-induced ALI models.[13] Notably, XFBD treatment has demonstrated therapeutic effects through the programmed cell death protein 1/interleukin (IL)-17A pathway, highlighting its potential in mitigating hyperinflammatory responses associated with COVID-19 and other respiratory conditions.[14] Furthermore, clinical trials have shown that XFBD can restore normal levels of leukocytes and lymphocytes.[15] In combat against the COVID-19 outbreak in China, XFBD intervention (lung ventilation and detoxification) has shown the effective prevention of disease progression. Clinical trials also revealed XFBD-mediated enhancement in clinical manifestations and immune metrics in patients with COVID-19 when it was used in conjunction with traditional medications, thereby diminishing the likelihood of disease advancement from a mild to a severe state.[16] Nonetheless, studies reporting a comprehensive understanding of molecular mechanisms associated with XFBD remain lacking.

The active ingredients in TCM form the pharmacological basis of their therapeutic effects. Previously, various active components of the prescription were isolated and purified, with studies reporting their main mode of action via the activation of endogenous receptors. For instance, many studies have reported certain active components of Chinese herbal medicine exhibiting phytoresolvin activities. Previously, we have isolated several phytoresolvin active components and showed their protective effects against sepsis and organ damage.[17] Among these components, liriodendrin and syringaresinol have shown considerable protective effects against organ damage, particularly sepsis-induced damage in the lungs. These compounds achieve their corresponding effects by inhibiting the nuclear factor (NF)-κB signaling pathway, thereby suppressing acute inflammatory responses.[18] Additionally, 3,4-dihydroxyphenylethanol glycoside has been shown to regulate macrophage polarization and inhibit sepsis-induced ALI, demonstrating its effectiveness.[19] Reportedly, the CCAAT/enhancer binding protein (C/EBP) plays a crucial role in recruiting and activating immune cells in the lung tissues by promoting the synthesis of pro-inflammatory cytokines, chemokines, and adhesion molecules.[20] Based on our previous studies, we observed a significant correlation between the activation of C/EBP-δ and the exacerbation of lung inflammation and injury during LPS-induced ALI.[21] Furthermore, the activein of the herb Verbenalin has been shown to activate the resolvin receptor GPR18, thereby reducing C/EBP-δ expression and alleviating acute inflammatory responses.[9] Hence, we hypothesize that GPR18 activation may contribute to the potential protective effects of XFBD against sepsis-induced ALI, playing a role similar to "plant resolvins." Based on our previously reported preliminary experimental results, we investigated the pivotal regulatory role of XFBD in sepsis-induced ALI/ARDS.

METHODS

Prediction of Active Ingredients of XFBD. We utilized the Traditional Chinese Medicine Systems Pharmacology Database and Analysis Platform (TCMSP) (http://tcmspw.com/index.php) to search for active compounds within XFBD. A total of 13 medicinal herbs and natural materials were included, namely: *Semen Armeniacae* Amarum from *Prunus sibirica* L., *Verbenae Herba* from *Verbena officinalis* L., *Ephedrae herba* from *Ephedra sinica* Stapf, and *Atractylodis Rhizoma* from *Atractylodes chinensis* (DC.) Koidz, *Glycyrrhizae Radix et Rhizoma* from *Glycyrrhiza uralensis* Fisch., and *Descurainiae Semen* from *Descurainia sophia* (L.) Webb. ex Prantl., *Polygoni Cuspidati Rhizoma et Radix* from *Polygonum cuspidatum* Siebold & Zucc., *Phragmitis Rhizoma* from *Phragmites communis* Trin., *Coicis Semen* from *Coix lacryma-jobi* L. var. *mayuen* (Roman.) Stapf, *Citri Grandis Exocarpium* from *Citrus grandis* (L.) Osbeck, *Artemisia annua Herba* from *Artemisia annua* L., *Pogostemonis Herba* from *Pogostemon cablin* (Blanco) Benth., and *Gypsum Fibrosum*.

Compounds with a drug-likeness (DL) of ≥0.18 and oral availability (OB) of ≥30% were considered as active ingredients. The relevant literature reports were combined with the active ingredients retrieved from the TCMSP platform.

Molecular Docking. Molecular docking analysis was conducted using SDF files of effective component targets retrieved from the PubChem and TCMSP databases. The PDB file of GPR18 was acquired from the AlphaFold Protein Structure Database. For the docking investigation, AutoDock Vina Extended was utilized to examine the most elevated binding energy and generate associated docking diagrams.

Reagents and Materials. The XFBD powder used in this study was obtained from the Tianjin Modern TCM Innovation Center (Batch No: XF210204). The production process involved soaking the 13 TCM ingredients (Lepidium apetalum Willd included in the prescription) in water in a 1:4 ratio for 30 min. This mixture was then brought to a boil and sustained at a high temperature for 40 min. Subsequently, the decoction

https://doi.org/10.1021/acsomega.4c10575
ACS Omega 2025, 10, 13105−13121

was filtered, and the resultant liquid was concentrated to achieve a relative density of 1.02−1.10 at 60 °C. Before administration, the extract was analyzed by high-performance liquid chromatography (HPLC) to confirm its composition. The standard samples of amygdalin, verbenin, naringin, and glycyrrhetinic acid were purchased from the National Institute for Inspection and Research of Pharmaceutical and Biological Products of China (Beijing, China). HPLC-grade acetonitrile, methanol, and formic acid were purchased from Xiehe Technology Co., Ltd. (Tianjin, China). The water used was ultrapure. LPS was purchased from Sigma-Aldrich Trading Co., Ltd. (MO, USA). Dulbecco's modified Eagle's medium (DMEM) and fetal bovine serum (FBS) were purchased from TransGen Biotech Co., Ltd. (Beijing, China). The 2× Universal Blue SYBR Green qPCR Master Mix was supplied by Servicebio (Wuhan, China), while PerfectStart Green qPCR SuperMix, containing both Dye I and Dye II, was obtained from TransGen Biotech. A GAPDH monoclonal antibody was obtained from Abcam (Cambridge, UK). Goat antimouse IgG (H + L) HRP and goat antirabbit IgG (H + L)/HRP were sourced from Huabio (Hangzhou, China). C/EBPδ antibody (C-6) was acquired from Santa Cruz Biotechnology (Texas, USA), and Caspase-1 (E9R2D) Rabbit mAb, ASC/TMS1 (D2W8U) Rabbit mAb, Cleaved Gasdermin D (Asp276) (E3E3P) Rabbit mAb, Gasdermin D (E9S1X) Rabbit mAb, NF-κB p65 (D14E12) XP Rabbit mAb, Toll-like Receptor 4 (D8L5W) Rabbit mAb, and Phospho-NF-κB p65 (Ser536) (93H1) Rabbit mAb were all procured from Cell Signaling Technology (Massachusetts, USA). Finally, the Mouse IL-1β ELISA Kit, Mouse IL-6 ELISA Kit, Mouse IL-18 ELISA Kit, and Mouse TNF-α ELISA Kit were purchased from Ruixinbio (Quanzhou, China).

Conditions of HPLC. XFBD (1 g) lyophilized powder was dissolved in 250 mL of ultrapure water and subjected to ultrasonic dissolution for 20 min. A 100 mL aliquot was extracted and diluted with methanol in an equal ratio. The mixed solution was then centrifuged at 14,000 rpm for 10 min. The supernatant was filtered through a 0.22-μm membrane filter. The filtered supernatant was analyzed by HPLC for the identification of various components in the XFBD. All separation operations were performed on the ZORBAX SB-C18 column (250 × 4.6 mm, 5 μm, Agilent Technologies). The detection wavelength was set at 254 nm; the flow rate was 1.0 mL/min; and the column temperature was maintained at 35 °C. The mobile phase was composed of 0.1% formic acid (A) and acetonitrile (B), with a gradient elution program of 5% B to 50% B from 0 to 50 min.

CLP Model and Experimental Protocol. Male C57BL/6 mice aged 6−8 weeks, free from specific pathogens, were obtained from Beijing Huafu Biotechnology Co., Ltd. (Beijing, China) and housed in a pathogen-free environment. All experimental procedures were approved by the Animal Care and Use Committee of the Tianjin University of Nankai Hospital (approval number NKYY-DWLL-2023-039). The research followed protocols outlined by the Animal Ethics Committee of the Nankai Hospital in Tianjin, China. The freeze-dried powder of XFBD was provided by the Tianjin Modern Traditional Chinese Medicine Innovation Center (TRT, 200302). XFBD extraction and raw material processing were carried out according to a previously published protocol. Briefly, the mice were assigned to five groups of 5 mice each in a randomized manner: the Sham group (sham-operated mice), the CLP group (mice subjected to the cecal ligation and puncture model), the CLP + XFBD-L group (mice treated with a low dosage of XFBD following the CLP model), the CLP + XFBD-H group (mice treated with a high dosage of XFBD post-CLP induction), and the CLP + XFBD-H + O1918 group (mice subjected to the CLP model and treated with high-dose XFBD alongside a GPR18 inhibitor). The Sham-operated mice underwent laparotomy without ligation or puncture. The ALI model induced by CLP was treated as per a previously published protocol. At the 6-h mark, the mice in the XFBD-L group received the XFBD solution via gavage at a concentration of 4 g/kg, while those in the XFBD-H group were administered the XFBD solution at a concentration of 8 g/kg via gavage. The calculation of the XFBD dosage for mice was based on clinical standards, where the total weight of all granules (29.988 g) was divided by 70 kg (the standard human body weight) and then multiplied by the conversion coefficient (9.1 for human-to-mouse conversion), yielding a dosage of 4 g/kg/day. After induction of ALI for 24 h, the mice were anesthetized and the blood serum and lung tissues were collected for experimental analyses.

Preparation of Serum-Containing XFBD. For our preparations, we produced serum infused with XFBD (XFBDs) and control serum (CONs). A total of 20 male Wistar rats weighing 180−200 g were arbitrarily assigned to two groups: CONs and XFBDs, with 10 rats in each group. The rats were intragastrically administered at a dose of 4 g/kg twice daily for 3 consecutive days as the mice in the XFBDs group, while an equivalent volume of water was provided to the CONs group. Following anesthesia, blood samples were collected from the abdominal aorta after 3 days, and the serum was obtained via centrifugation at 3000 rpm for 10 min. Following a water bath treatment at 56 °C for 30 min, the serum was filtered using a 0.22-μM filter membrane, and the aliquoted filtered serum was stored at −80 °C. CONs at 10 and 20% concentrations, as well as XFBDs at 10 and 20% concentrations, were individually introduced into macrophage experiments.

In Vitro Cell Culture with Subsequent LPS Treatment. Mouse alveolar macrophages (MH-S cells) were obtained from The Cell Bank of the Chinese Academy of Sciences located in Shanghai, China, for the experiments. Under 5% CO2, the MH-S cells were maintained at 37 °C, supplemented with 5% inactivated FBS and 1640 medium, and cultivated in cell-culture plates. The cells were stimulated with LPS at a concentration of 100 ng/mL for 24 h following a 1-h treatment with XFBDs and O1918.

Flow Cytometry Analysis. The obtained mouse spleen tissues were subjected to sectioning by using scissors. The tissue sections were then ground into single cells using a cell sieve. In the PBS solution, the cells were resuspended after red blood cell lysis and stained with F4/80-APC, anti-CD11b-FITC, and anti-CD86-PE in the dark at 4 °C for 30 min. Following this, the cells were washed three times with the staining buffer suspension in 200 μL of PBS for examination by the NovoCyte Flow Cytometer (Dakewe Biotech Co., Shenzhen, China). The data obtained from the experiment were processed and interpreted by using the NovoCyte flow software.

Quantitative Real-Time PCR (qPCR). RNA extraction was performed on MH-S cells and mouse lung tissues by using an RNA extraction reagent sourced from TransGen Biotech. Subsequently, the RNA underwent reverse transcription into cDNA by using a reverse transcription kit, in accordance with

https://doi.org/10.1021/acsomega.4c10575
ACS Omega 2025, 10, 13105−13121

Table 1. Sequences of Primers Used for qPCR

gene	forward (5′-3′)	reverse (5′-3′)
IL-6	GAGGATACCACTCCCAACAGACC	AAGTGCATCATCGTTGTTCATACA
IL-1β	GCCACCTTTTGACAGTGATGAG	ATGTGCTGCTGCGAGATTTG
TNF-α	GCGCCAAGCATTCAATGAGC	ATCTCTTCCCCACCCCGAAT
IL-18	GTGAACCCCAGACCAGACTG	CCTGGAACACGTTTCTGAAAGA
GAPDH	GCCTCGTCTCATAGACAAGATG	CAGTAGACTCCACGACATAC

the manufacturer's guidelines. For the qPCR analysis of IL-6, IL-1β, and TNF-α mRNA expressions, a SYBR Mix (Yeasen, Shanghai, China) was used. The mRNA expressions were normalized to GAPDH as a reference. The details of the primer sequences used in the study are available in Table 1.

Western Blotting Analysis. For a duration of 30 min, lung tissues and MH-S cells were lysed in RIPA lysis buffer containing phosphatase and protease inhibitors. Following quantification using a BSA kit, 40 μg of protein was subjected to SDS-PAGE for separation and subsequent transfer onto a PVDF membrane. Following a 90 min blocking step with 5% skim milk at the ambient temperature, the PVDF membrane was horizontally divided based on the molecular weight of the antibodies. On the following day, the membranes were treated with HRP-conjugated secondary antibodies at room temperature for 2 h. The visualization of antibody binding was accomplished using ECL. The primary antibodies used in the study included NF-κB, P-NF-κB, C/EBP-δ, ASC, NLRP3, Caspase-1, GSDMD, cleaved-GSDMD, and GAPDH.

Enzyme-Linked Immunosorbent Assay (ELISA). The serum was collected after the aforementioned experiment was replicated with five mice in each group. ELISA kits were used to assess the secretion levels of IL-6, IL-1β, and TNF-α in both the serum and cell supernatant, in accordance with the manufacturer's guidelines. The Microplate Reader 1500 (Thermo Fischer) was used to measure the absorbance at 450 nm.

Detection of Blood Endotoxin. Serum samples were collected from mice after surgery by using pyrogen-free tubes. Endotoxin levels in the serum were then measured following the manufacturer's instructions with an End-point Chromogenic *Tachypleus amebocyte* Lysate kit (Xiamen Bioendo Technology Co., Ltd.). The endotoxin concentration was determined by calculating the absorbance at 405 nm using an ELISA reader and referencing a standard curve.

Hematoxylin and Eosin. At the 24-h mark following CLP induction, the samples of lung and colon tissues underwent fixation with 4% para-formaldehyde. Subsequently, they were subjected to dehydration, followed by embedding in paraffin and slicing into serial sections of 5-μm thickness. These sections were then subjected to hematoxylin and eosin (H&E) staining and examined under a light microscope for visualization.

MPO Analysis. The assessment of the MPO activity in the lung tissues was conducted using an MPO assay kit (Nanjing Jiancheng Bioengineering Institute, China). First, the lung tissues were homogenized in an extraction buffer provided by the manufacturer. Following homogenization, the homogenate or serum was mixed with the reaction solution and allowed to incubate at 37 °C for 30 min. Subsequently, the mixture was subjected to incubation at 60 °C for 10 min, followed by the addition of 50 μL of hydrogen peroxide. The absorbance of the resultant mixture was measured at 460 nm using a multimode microplate reader. One unit of MPO activity was defined as the

Table 2. Docking Results of XFBD Active Ingredients with GPR18

active ingredient	docking score (kcal/mol)
3-phenylpropyl acetate	−7.9
beta-carotene	−7.8
cholesterol	−7.8
sitosterol	−7.6
diisooctyl phthalate	−7.4
campest_5_en_3beta_ol	−7.4
poriferast_5_en_3beta_ol	−7.4
daucosterol_qt	−7.3
stigmasterol 3-O-beta-D-glucopyranoside_qt	−7.3
carboxylic acid	−7.2
spinasterol	−7.1
supraene	−7
glabridin	−7
hexaene	−7
phaseol	−7
ziziphin_qt	−6.9
LYC	−6.8
licochalcone B	−6.8
estrone	−6.7
carboxylic	−6.7
torachrysone-8-O-beta-D-(6'-oxayl)-glucoside	−6.6
SPD	−6.6
isosinensetin	−6.5
sinensetin	−6.5
cornudentanone	−6.5
dihydroverticillatine	−6.5
enoate	−6.5
dimethoxyflavanon	−6.4
trimethylapigenin	−6.4
nobiletin	−6.4
areapillin	−6.4
artemisitene	−6.4
deoxyartemisinin	−6.4
eicosadienoic acid	−6.4
gondoicacid	−6.4
machiline	−6.4
Mairin	−6.4
NSC63551	−6.4
Wogonin	−6.4
Genkwanin	−6.3
24_Ethylcholest-4-en-3-one	−6.3
Artemisinin	−6.3
Skrofulein	−6.3
diisooctylsuccinate	−6.3
daucosterin_qt	−6.3
3,23-dihydroxy-12-oleanen-28-oic acid	−6.2
didymin	−6.2
neohesperidin_qt	−6.2
mandenol	−6.2
pectolinarigenin	−6.2

https://doi.org/10.1021/acsomega.4c10575
ACS Omega 2025, 10, 13105−13121

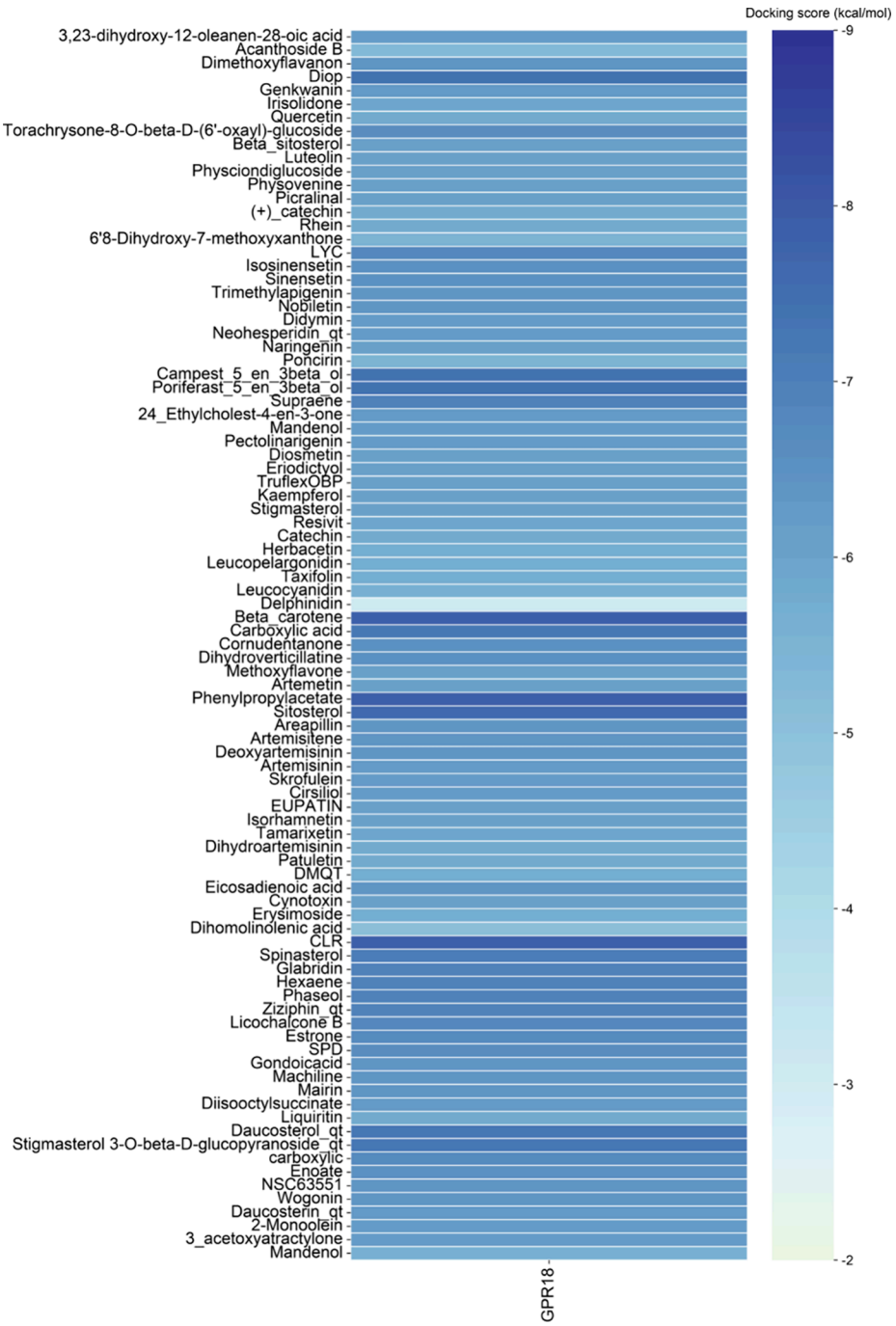

Figure 1. Top 50 degree-ranked targets and molecular docking results with GPR18.

amount of enzyme capable of decomposing 1 micromol of hydrogen peroxide at 37 °C. The outcomes were quantified as units per gram of the lung tissues.

Fecal Microbiota Analyses. Fecal sample DNA was extracted using the FastDNA Stool Mini Kit (Qiagen) in accordance with a previously provided protocol. The V3−V4 region of the bacterial 16S rRNA gene was amplified with universal primers, and the resulting barcoded amplicons were pooled in equal concentrations for sequencing on the Illumina MiSeq platform with MiSeq Reagent Kit v.3. Raw sequence data were preprocessed by using Trimmomatic to remove low-quality reads and adapters. Taxonomic classification was performed using QIIME 2 with the Silva database, and the DADA2 algorithm was employed for read demultiplexing, error correction, and chimera removal. Diversity analyses were conducted to evaluate the microbial composition, with alpha diversity assessed via the Shannon index and beta diversity visualized through the PCoA plots based on Bray−Curtis and weighted UniFrac distances, using QIIME 2 plugins and the qiime2R package.

Statistical Analyses. The results incorporated data presented as the means ± SEM and were analyzed using GraphPad Prism 8 (GraphPad Software, USA). Group comparisons were executed via one-way analysis of variance (ANOVA). A significance threshold of $P < 0.05$ was applied to determine the statistical significance.

https://doi.org/10.1021/acsomega.4c10575
ACS Omega 2025, 10, 13105−13121

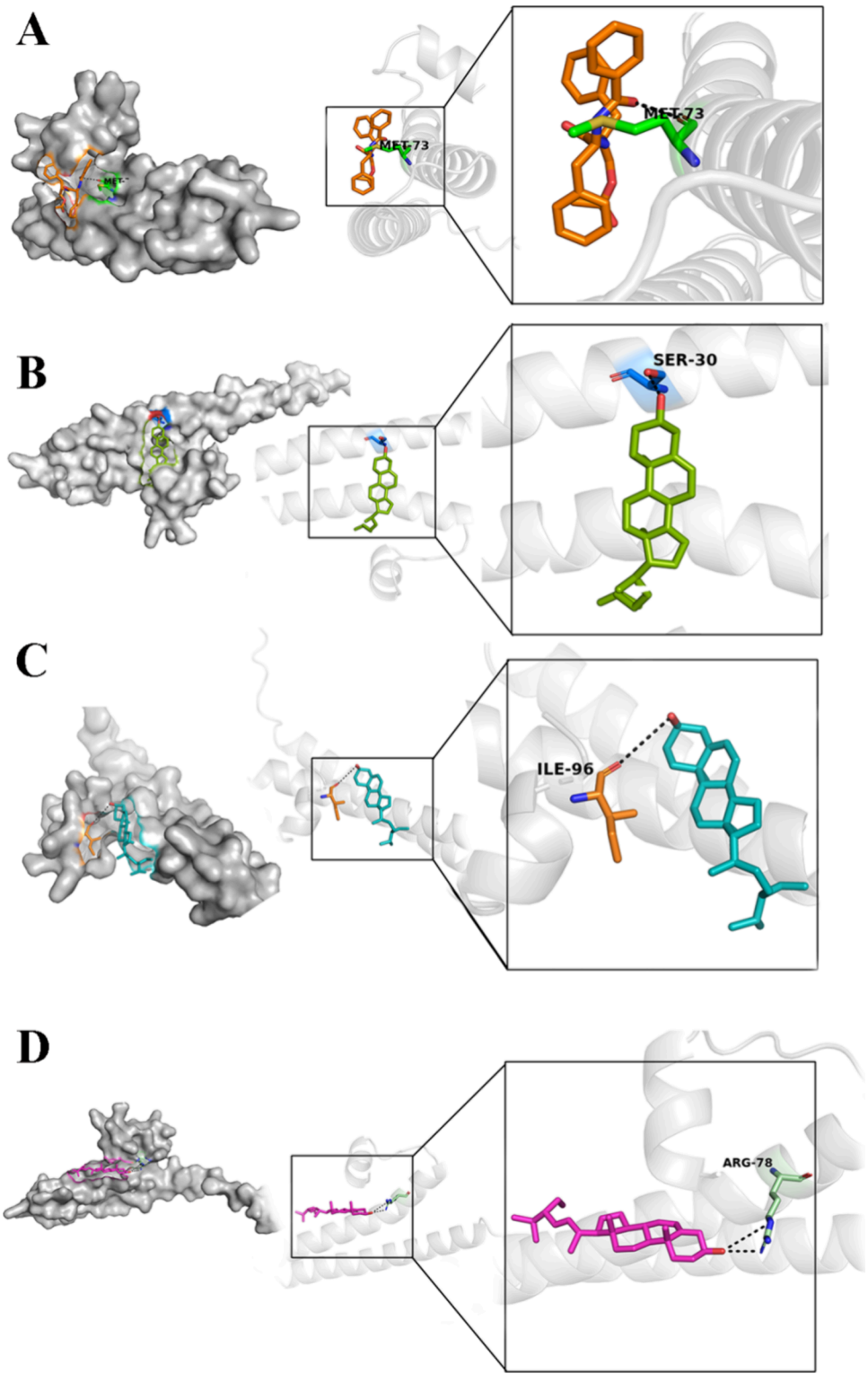

Figure 2. Molecular docking results of the top four ranked docking scores: (A) 3-phenylpropyl acetate docking with GPR18; (B) beta-carotene docking with GPR18; (C) cholesterol docking with GPR18; (D) sitosterol docking with GPR18.

RESULTS

Molecular Docking Validation of Core Active Ingredients in XFBD. Molecular docking was performed for 91 core ingredients in XFBD with GPR18, and the top 50 results are presented in Table 2. Notably, the core active ingredients in XFBD generally exhibited binding energies of less than −5 kcal/mol with GPR18, indicating spontaneous and favorable interactions between them. Figure 1 graphically illustrates the docking results for 50 core chemical components with GPR18, along with the minimum binding energies. On the horizontal axis, the target protein GPR18 is depicted, whereas the active ingredients of XFBD are on the vertical axis. The color intensity represents the magnitude of the minimum binding energy. Figure 2 presents the docking results of the top four

https://doi.org/10.1021/acsomega.4c10575
ACS Omega 2025, 10, 13105−13121

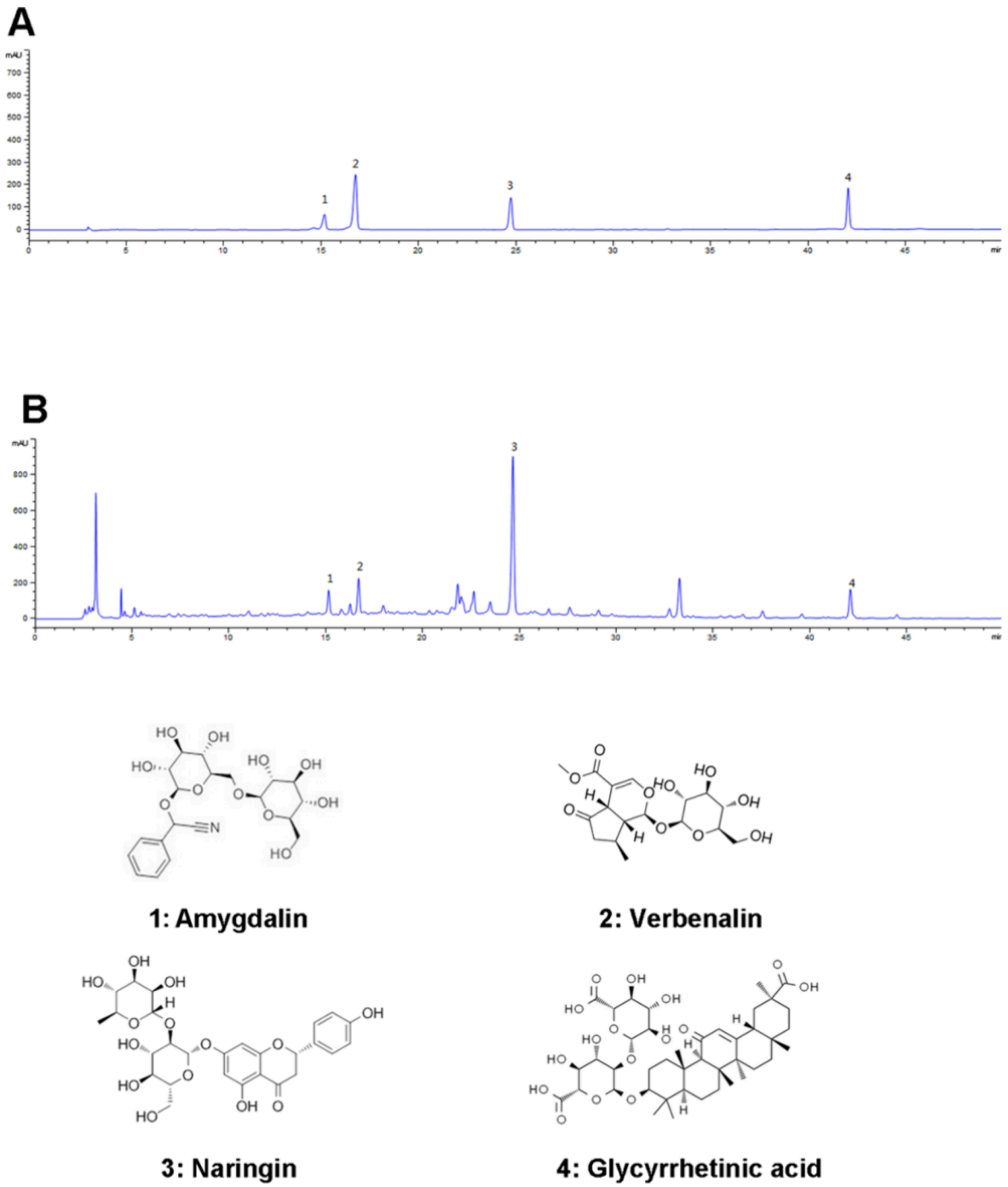

Figure 3. Results of XFBD component analysis by HPLC. (A) Chromatogram of a standard mixture XFBD, peak 1: amygdalin, peak2: verbenalin, peak 3: naringin, peak 4: glycyrrhetinic acid. (B) XFBD components, peak 1: amygdalin, peak2: verbenalin, peak 3: naringin, peak 4: glycyrrhetinic acid.

compounds ranked per their binding energies with GPR18. For instance, compounds such as 3-phenylpropyl acetate (Figure 2A), beta_carotene (Figure 2B), cholesterol (Figure 2C), and sitosterol (Figure 2D) formed one hydrogen bond each with GPR18.

Identification of the Chemical Components of XFBD by HPLC. The chemical composition of the XFBD extract was analyzed and identified through HPLC. The chromatogram of XFBD was separately obtained at 254 nm (Figure 3A). The four main active ingredients, namely, amygdalin, verbenin, naringin, and glycyrrhetinic acid, were identified through comparative reference standards (Figure 3B).

XFBD Mitigated CLP-Induced ALI By Activating GPR18. The components of XFBD have been delineated previously through an ultra-HPLC-photo diode array.[22] The present study aimed to assess whether XFBD could alleviate CLP-induced lung injury. Notably, the results of pathological examinations showed that the lungs of mice in the control group exhibited a typical structural pattern devoid of any indications of inflammatory responses (Figure 4A,B). Conversely, CLP mice displayed evident pulmonary inflammation

https://doi.org/10.1021/acsomega.4c10575
ACS Omega 2025, 10, 13105−13121

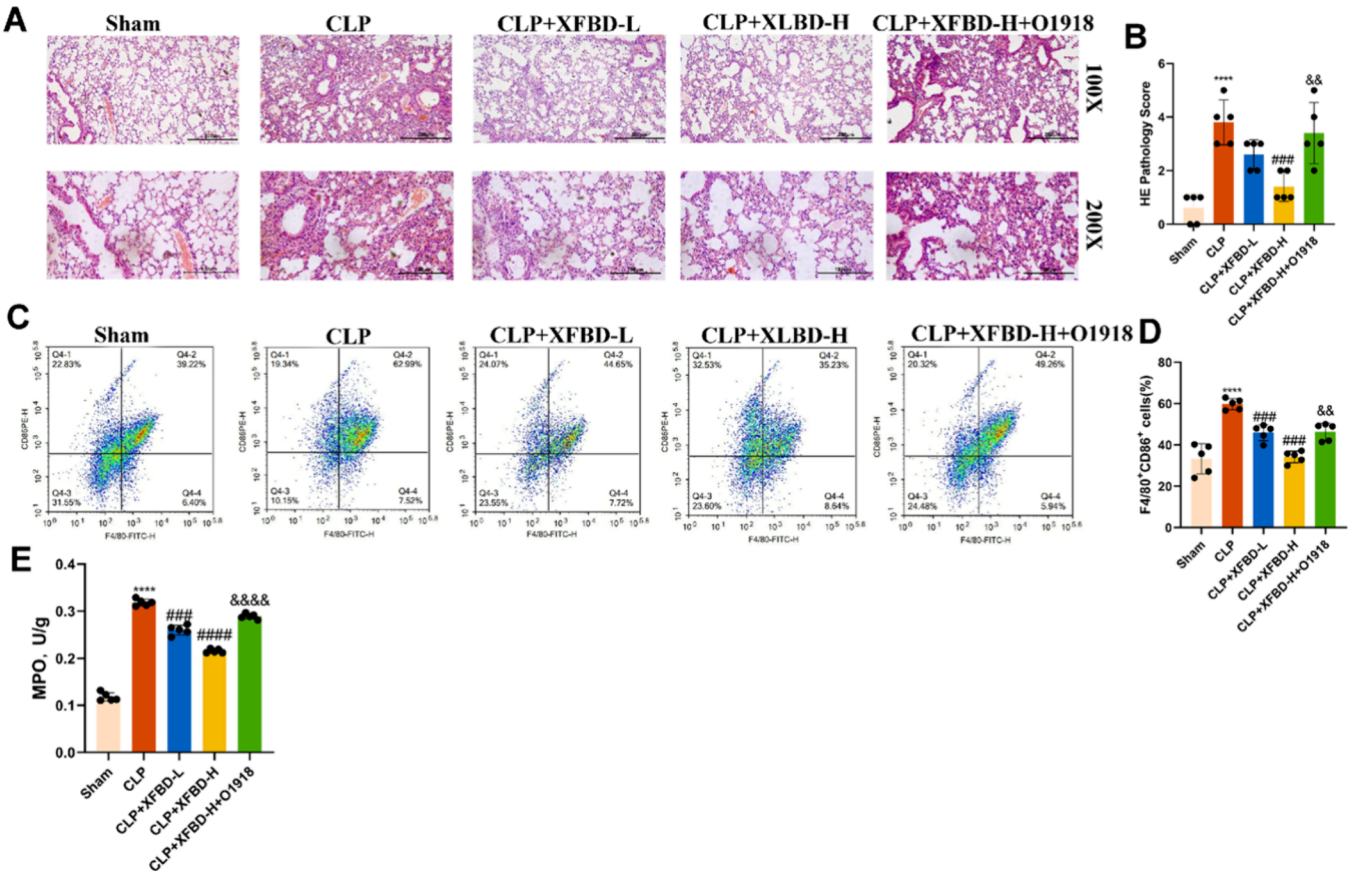

Figure 4. XFBD alleviated pathological damage in a mouse model of ALI induced by CLP, and the GPR18 inhibitor eliminated the anti-inflammatory response. (A) Lung tissue histopathological damage 24 h after CLP modeling evaluated by H&E staining, with images captured at 200× magnification. (B) Lung histopathology scores. (C) Proportion of F4/80$^+$ CD86$^+$ cells detected by flow cytometry in the spleens of CLP mouse models treated with PBS (control) or XFBD decoction. (D) The effect of XFBD on the MPO expression in the mouse model induced by CLP. All image data shown are representative of the experimental results. $^{****}P < 0.0001$ compared with the Sham group, $^{\#\#\#}P < 0.001$ compared with the CLP group, $^{\&\&}P < 0.01$ compared with the CLP + XFBD-H group.

features including inflammatory cell infiltration, hemorrhage, alveolar space enlargement, and thickening of alveolar walls. Compared with the CLP mice group, both XFBD-L and XFBD-H treatment groups exhibited a notable reduction in CLP-induced tissue inflammatory features, whereas adding GPR18 inhibitor, O1918 reversed the protective effect of XFBD treatment.

To further elucidate the effects of XFBD on macrophages and their different subgroups in the CLP-induced ALI mice model, flow cytometry analysis was performed for macrophages derived from the spleen along with their distinct phenotypic expressions. In the CLP groups, flow cytometry revealed an increased percentage of F4/80$^+$ CD11b$^+$ CD86$^+$ M1 macrophages in the spleen, which were identified as classically activated (M1). Nevertheless, the administration of high-dose XFBD markedly reduced the proportion of M1 macrophages (Figure 4C,D), and the addition of the GPR18 inhibitor O1918 reversed this effect. Additionally, both XFBD-L and XFBD-H treatment groups exhibited considerable reductions in the tissue levels of MPO induced by CLP, which were negated in the O1918 treatment group (Figure 4E).

XFBD Inhibited the Activation of the NF-κB Signaling Pathway and C/EBP-δ in CLP-Induced ALI. The overexpression of various pro-inflammatory mediators substantially contributes to CLP-induced ALI. Hence, the effects of XFBD on CLP-mediated production of pro-inflammatory factors were investigated. Notably, LPS, IL-1β, IL-6, and TNF-α exhibited a marked increase in their expression in peripheral blood triggered by CLP (Figure 5A). Conversely, the XFBD-L and XFBD-H groups suppressed the increase in the expression of these factors. Conversely, the GPR18 inhibitor restored the expression of pro-inflammatory factors.

To further elucidate the correlation of XFBD-mediated suppression of pro-inflammatory cytokine generation with the modulation of the C/EBP-δ and NF-κB signaling cascades, Western blotting was performed. The results facilitated scrutinization of the levels of P-NF-κB, NF-κB, toll-like receptor (TLR)4, and C/EBP-δ proteins within lung tissues. Notably, in the lung tissues of CLP-induced mice, C/EBP-δ, TLR4, and P-NF-κB levels exhibited a considerable increase, as revealed by immunoblot analysis (Figure 5B). In the XFBD-H group, the expression of C/EBP-δ, TLR4, and P-NF-κB markedly decreased in the lung tissues compared to that in the CLP-induced group. Interestingly, the addition of the GPR18 inhibitor O1918 reversed these effects of XFBD, and the expression of TLR4 did not change with the addition of the inhibitor O1918.

Effects of XFBD on NLRP3 Inflammasome-Dependent Pyroptosis and CLP-Induced ALI In Vivo. Herein, we evaluated the effects of XFBD on pyroptosis in CLP-induced mice to explore the potential mechanisms underlying the

https://doi.org/10.1021/acsomega.4c10575
ACS Omega 2025, 10, 13105−13121

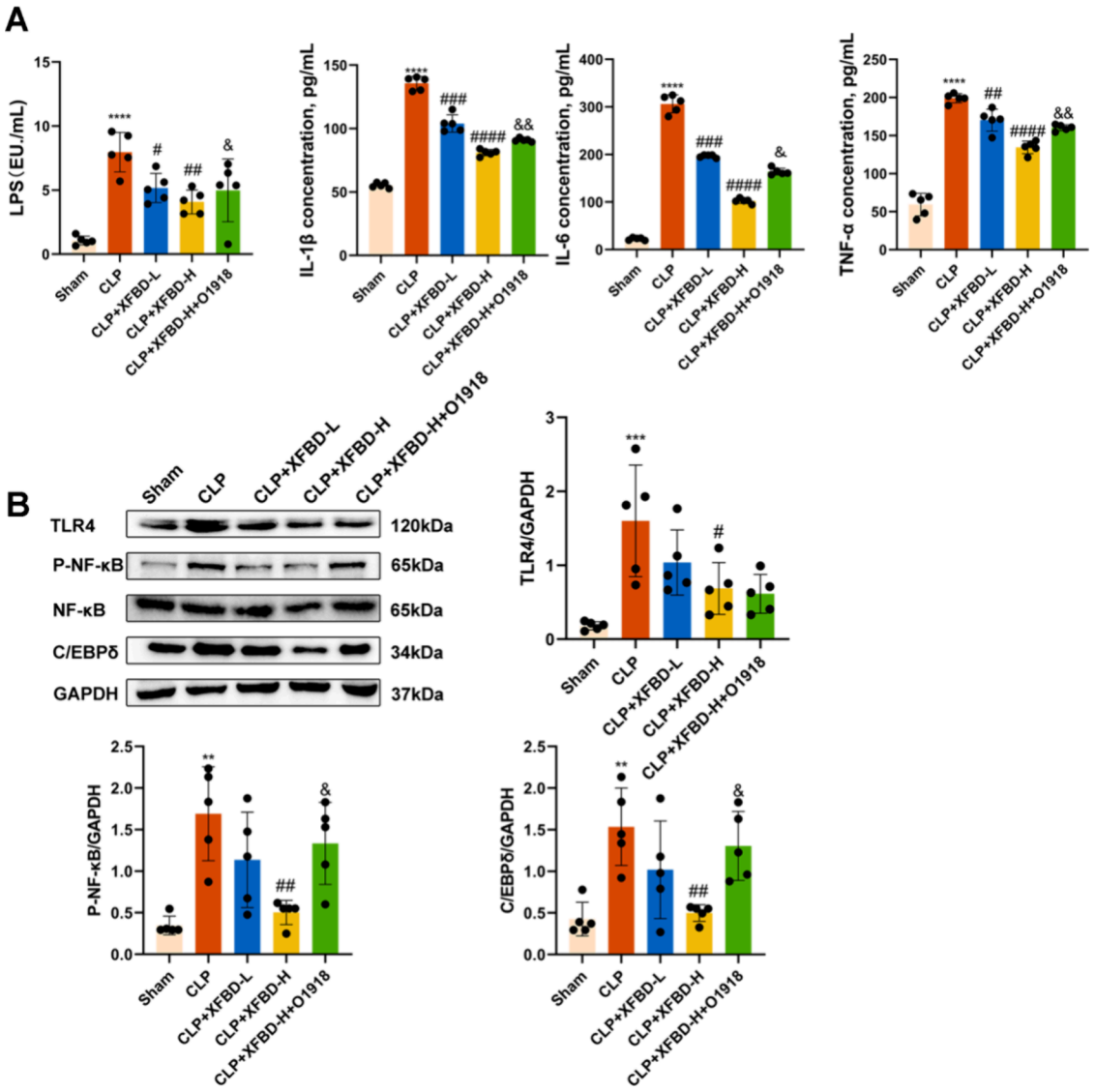

Figure 5. Alleviating effect of the selective GPR18 agonist XFBD on CLP-induced ALI mice. (A) Levels of LPS, TNF-α, IL-1β, and IL-6 in peripheral blood were detected by ELISA. (B) Western blotting exhibits the expression of TLR4, P-NF-κB, NF-κB, and C/EBPδ proteins in the lung tissues. The data presented in Figure 9A,B represent the mean ± SEM of five independent experiments. $^{**}P < 0.01$ when compared with the Sham group, $^{****}P < 0.0001$ when compared with the Sham group, $^{\#\#}P < 0.01$ when compared with the CLP group, $^{\#\#\#}P < 0.001$ when compared with the CLP group, $^{\#\#\#\#}P < 0.001$ when compared with the CLP group, $^{\&}P < 0.05$ when compared with the CLP + XFBD-H group, $^{\&\&}P < 0.01$ when compared with the CLP + XFBD-H group.

XFBD-mediated protective effect against CLP-induced ALI. Western blotting of the lung tissues of septic mice revealed that compared with the Sham group, ASC, Cleaved-GSDMD, NLRP3, GSDMD, and Caspase-1 levels were markedly increased in CLP-induced ALI, whereas the XFBD-H groups exhibited marked down-regulation of these proteins (Figure 6A). However, the addition of the GPR18 inhibitor O1918 restored the expression of these proteins. qPCR and ELISA results indicated a notable increase in IL-18 expression under CLP stimulation, which was considerably down-regulated under XFBD treatment. The addition of the GPR18 inhibitor O1918 restored IL-18 expression (Figure 6B,C).

Effects of XFBD on the Intestinal Barrier and Gut Microbiota in the CLP-Induced ALI Mice Model. Reportedly, CLP can trigger disturbances in the intestinal barrier and alter the gut microbiota, leading to bacterial relocation and ALI onset. Hence, we investigated the effects of XFBD on the integrity of the intestinal barrier and gut microbiota composition in CLP-induced mice.

Notably, the pathological examination results showed that the lungs of the control mice presented a typical structure devoid of any indications of inflammatory responses (Figure 7A). Conversely, CLP mice presented substantial colon tissue damage, including increased infiltration of inflammatory cells and a reduced number of crypts. Compared with the CLP group, both low- and high-dose XFBD treatment considerably reduced CLP-induced tissue inflammation, and the addition of the GPR18 inhibitor O1918 reversed this protective effect of XFBD treatment. Furthermore, we collected fecal samples from each group for 16S rRNA (rRNA) gene sequencing. Figure 7B,C illustrates the results of Alpha diversity analysis, indicating noteworthy differences between the model and control groups. Notably, the Richness and Chao1 indices in the model cohort exhibited a marked decline compared with

https://doi.org/10.1021/acsomega.4c10575
ACS Omega 2025, 10, 13105−13121

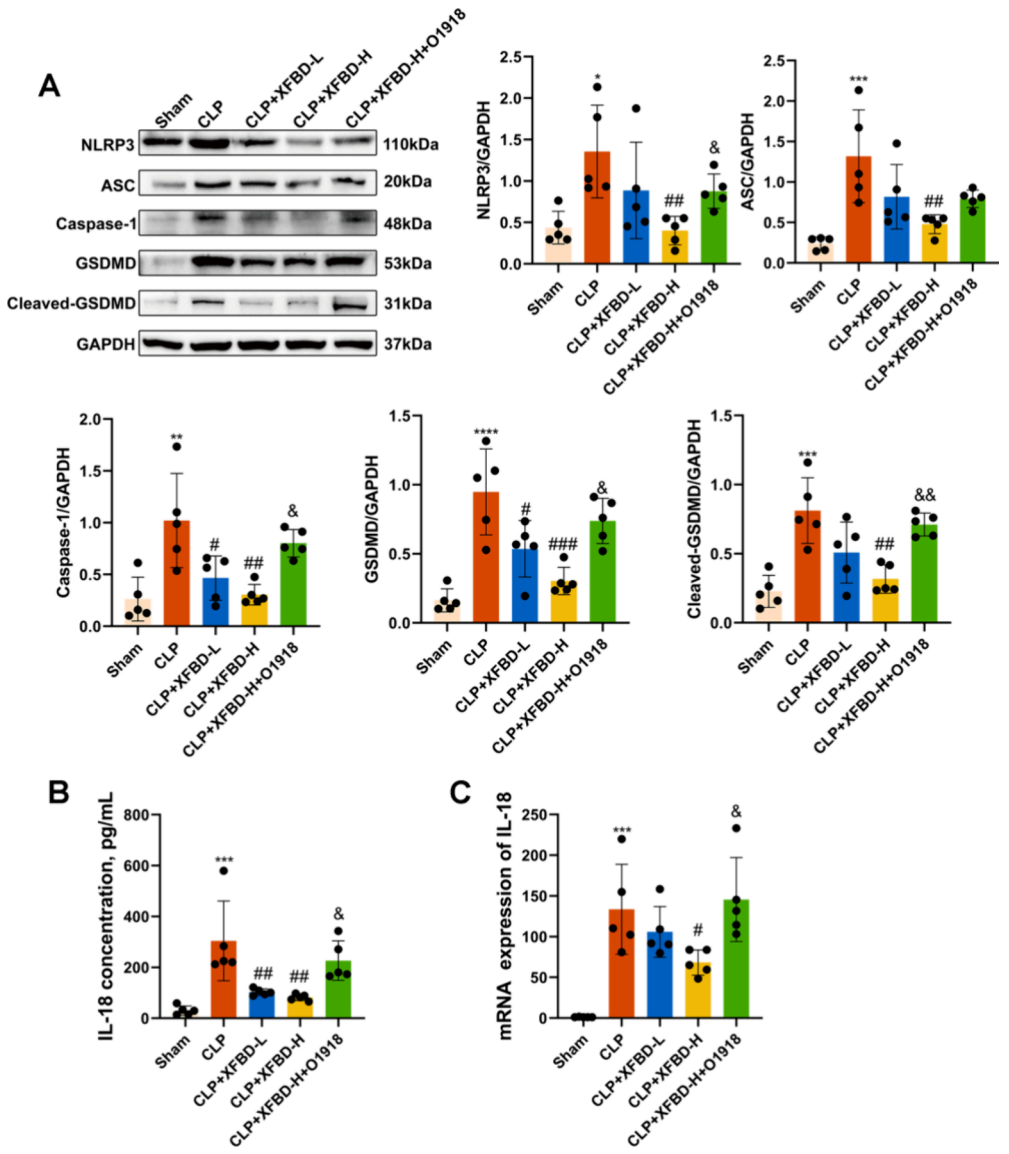

Figure 6. XFBD demonstrates the inhibition of GSDMD-mediated pyroptosis in ALI mice induced by IgG-IC, and the GPR18 inhibitor O1918 counteracted the antipyroptosis effect. (A) NLRP3, ASC, GSDMD, Cleaved-GSDMD, and Caspase-1 were detected by Western blotting. (B) ELISA detection of IL-18 concentrations in the serum. (C) qPCR assay detection of the IL-18 mRNA expressions in the lung tissues. Data are presented as the mean ± SEM for five independent experiments. $^{*}P < 0.05$ when compared with the Sham group, $^{**}P < 0.01$ when compared with the Sham group, $^{***}P < 0.001$ when compared with the Sham group, $^{****}P < 0.0001$ when compared with the Sham group, $^{\#}P < 0.05$ when compared with the CLP group, $^{\#\#}P < 0.01$ when compared with the CLP group, $^{\#\#\#}P < 0.001$ when compared with the CLP group, $^{\&}P < 0.05$ when compared with the CLP + XFBD-H group, $^{\&\&}P < 0.01$ when compared with the CLP + XFBD-H group.

those in the control cohort. This decline suggested that the species diversity of intestinal microbiota decreased in CLP-induced mice. After treatments with XFBD and O1918, the observed Richness and Chao1 indices increased, indicating the restorative effects of XFBD on species richness of the gut microbiota in CLP mice, and O1918 could not eliminate the effect of XFBD on the microbiota. To assess the Beta diversity of gut microbiota in each mouse group, a principal coordinated analysis was performed. The results showed notable differences in gut microbiota composition across groups, indicating that XFBD treatment can, to some extent, normalize the distribution of gut microbiota (Figure 7D).

Finally, linear discriminant analysis effect size was performed to identify species with significant differences from phylum to genus levels, and notable distinctions in the prominently enriched species among each respective group are presented in Figure 8A,B.

XFBD Inhibited the Signaling Pathway of C/EBP-δ and NF-κB in LPS-Stimulated Alveolar Macrophages. We assessed the potential of XFBD to alleviate LPS-induced inflammatory response in macrophages to further explore the in vitro effects of XFBD. Following a 1 h pretreatment with LPS, cells were incubated for 24 h with varying ratios of CONs or XFBD. Initially, the main focus was to evaluate the influence of XFBD on IgG-IC-induced production of pro-inflammatory mediators. ELISA results revealed a notable increase in the secretion of IL-6, IL-1β, and TNF-α under IgG-IC stimulation, which was blocked by 10% XFBD when compared with 10% CONs (Figure 9A). This finding is consistent with the in vivo results obtained in this study, which were reversed following the addition of the GPR18 inhibitor O1918. The results of

https://doi.org/10.1021/acsomega.4c10575
ACS Omega 2025, 10, 13105−13121

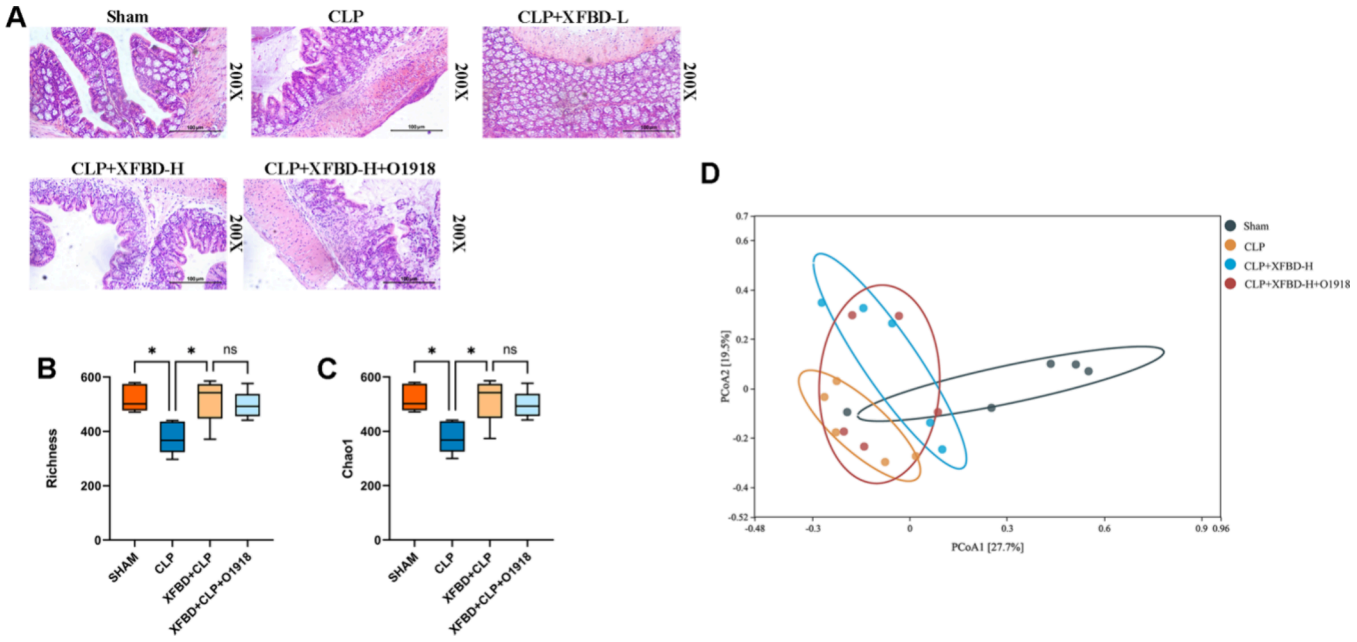

Figure 7. Effect of XFBD on the intestinal barrier and gut microbiota in mice with CLP-induced ALI. (A) Histopathological images of the colon tissues in each group. (B, C) Alpha diversity is illustrated using chao1 and Richness. (D) PCoA was used to analyze the bacterial communities of each group of β-diversity assessment. The significance of differences between the groups was evaluated using nonparametric factors Kruskal–Wallis and rank tests. *$P < 0.05$ is considered to indicate significant differences between the groups.

qPCR showed that CLP-induced expression of IL-1β, IL-6, and TNF-α was up-regulated, and compared with 10% CONs, the expression induced by 10% XFBD was markedly reduced (Figure 9B). After LPS stimulation, the activation of NF-κB led to the upregulation of multiple pro-inflammatory cytokines (including IL-6, TNF-α, and IL-1β). The GPR18 inhibitor O1918 effectively countered this effect, down-regulating these cytokines. Furthermore, LPS stimulation increased the expression of C/EBP-δ and P-NF-κB (Figure 9C). However, when 10% XFBDs were compared to 10% CONs, a notable reduction in their activity was observed, which was reversed following the addition of the GPR18 inhibitor O1918.

Effects of XFBD on NLRP3 Inflammasome-Dependent Pyroptosis In Vitro. Reportedly, XFBD can mitigate inflammatory reactions in IgG-IC-induced MH-S cells by suppressing the protein kinase B signaling pathway activation, thereby down-regulating mRNA levels of pro-inflammatory cytokines. Nonetheless, the involvement of XFBD in hindering NLRP3 inflammasome-dependent pyroptosis in LPS-induced cells remains elusive. Consistent with the in vivo results, the expression of relevant pyroptosis proteins markedly increased following LPS stimulation (Figure 10). The increase in NLRP3, ASC, Caspase-1, cleaved-GSDMD, and GSDMD protein expression was inhibited by 10% XFBDs, and the addition of a protein inhibitor, O1918, restored their expression. Overall, these findings indicate the potential of XFBD in mitigating inflammation through the inhibition of NLRP3 inflammasome-mediated pyroptosis in LPS-stimulated MH-S cells.

DISCUSSION

An excessive inflammatory response induced by a secondary cytokine storm is characteristic of COVID-19. XFBD has shown unique advantages in treating COVID-19, with a notable decline in the disease progression from mild to severe states. These advantages of XFBD suggest its protective application in alleviating inflammation. Reportedly, XFBD exhibits notable efficacy in the management of LPS- and IgG-IC-induced ALI.[23] Hence, the present study aimed to elucidate the notable inhibitory effects of XFBD on the progression of CLP-induced ALI. The results showed that XFBD can ameliorate lung injury by attenuating inflammatory cell infiltration and reducing MPO levels in lung tissues. Simultaneously, it modulates the M1 polarization of macrophages, thereby decreasing the release of inflammatory cytokines to safeguard lung tissue from harm. Furthermore, molecular docking results indicated that GRP18 is the main target of XFBD against ALI.

Activated transcription factors such as C/EBP-δ and NF-κB initiate a robust pro-inflammatory cascade reaction during CLP-induced ALI.[24] Herein, XFBD could inhibit the activation of the C/EBP-δ and NF-κB signaling pathways in lung tissues and macrophages, thereby reducing TNF-α, IL-6, and IL-1β levels. Additionally, pyroptosis has been reported to play a notable role in the development of sepsis-related ALI.[25] Moreover, confirmation of pyroptosis induction in patients with severe COVID-19 has been established, with excessive pyroptosis leading to the precipitation of a dysregulated host immune response, and thus, potentially resulting in organ dysfunction.[26] In this study, the results showed that sepsis can trigger NLRP3/ASC-dependent Caspase-1 activation and pyroptosis in MH-S cells. However, XFBD treatment inhibited the activation of NLRP3 inflammasomes, reducing the expression of key pyroptosis-related proteins and decreasing the secretion of IL-18 and IL-1β.

To explore the effects of XFBD on LPS-triggered inflammation and cell apoptosis in alveolar macrophages, serum application pharmacology in vitro was employed. Previously, we have shown that GPR18 activation could mitigate LPS-induced ALI by suppressing inflammatory signaling pathways and macrophage pyroptosis activation.[9] Both in vivo and in vitro investigations revealed that XFBD

https://doi.org/10.1021/acsomega.4c10575
ACS Omega 2025, 10, 13105−13121

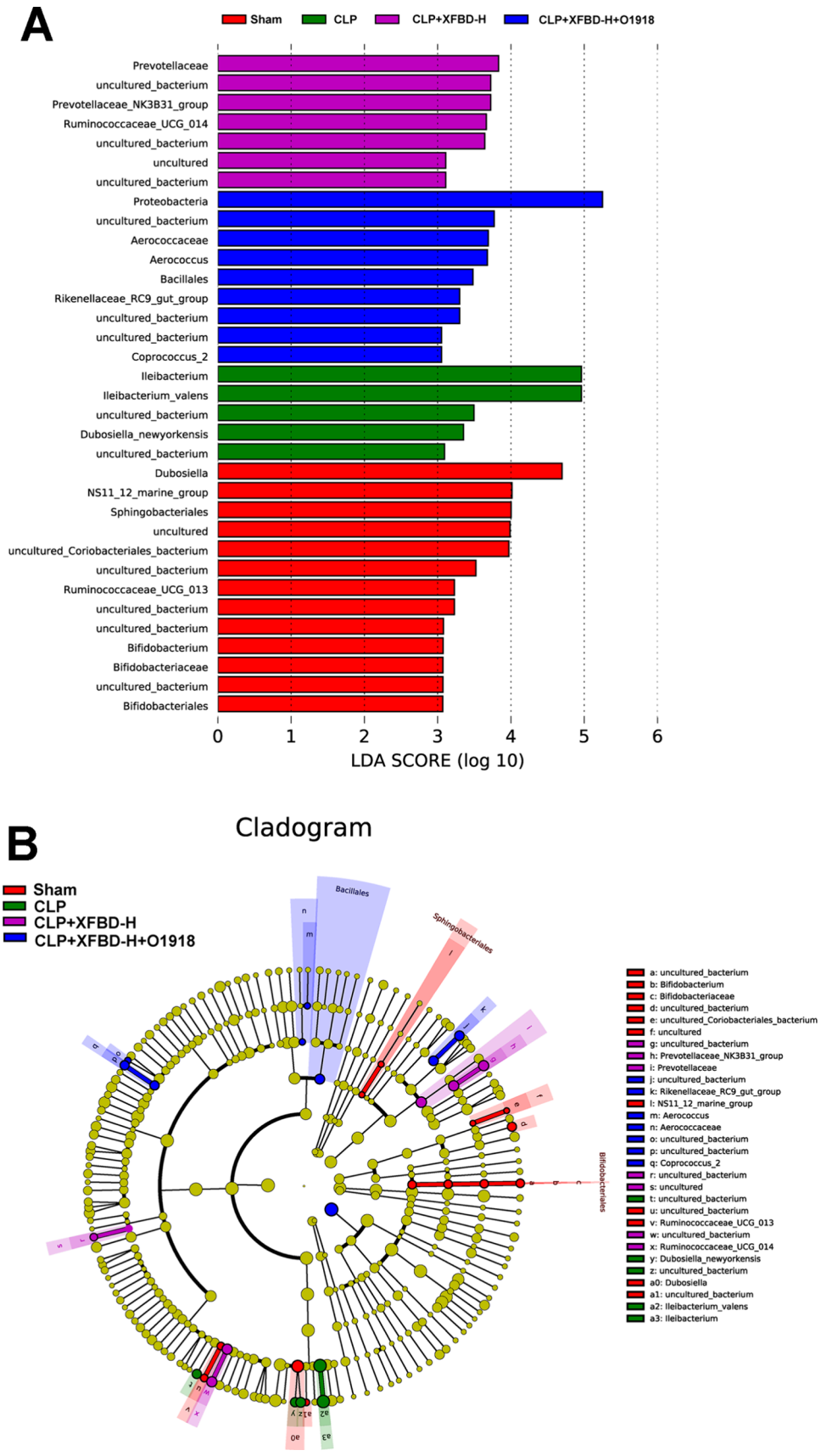

Figure 8. Gut microbiota composition and enrichment analysis across groups. (A) Branch diagram of the gut microbiota in each group. (B) LDA scores of significantly enriched gut microbiota were in each group. The significance of differences between the groups was evaluated using nonparametric factors Kruskal−Wallis and rank tests.

https://doi.org/10.1021/acsomega.4c10575
ACS Omega 2025, 10, 13105−13121

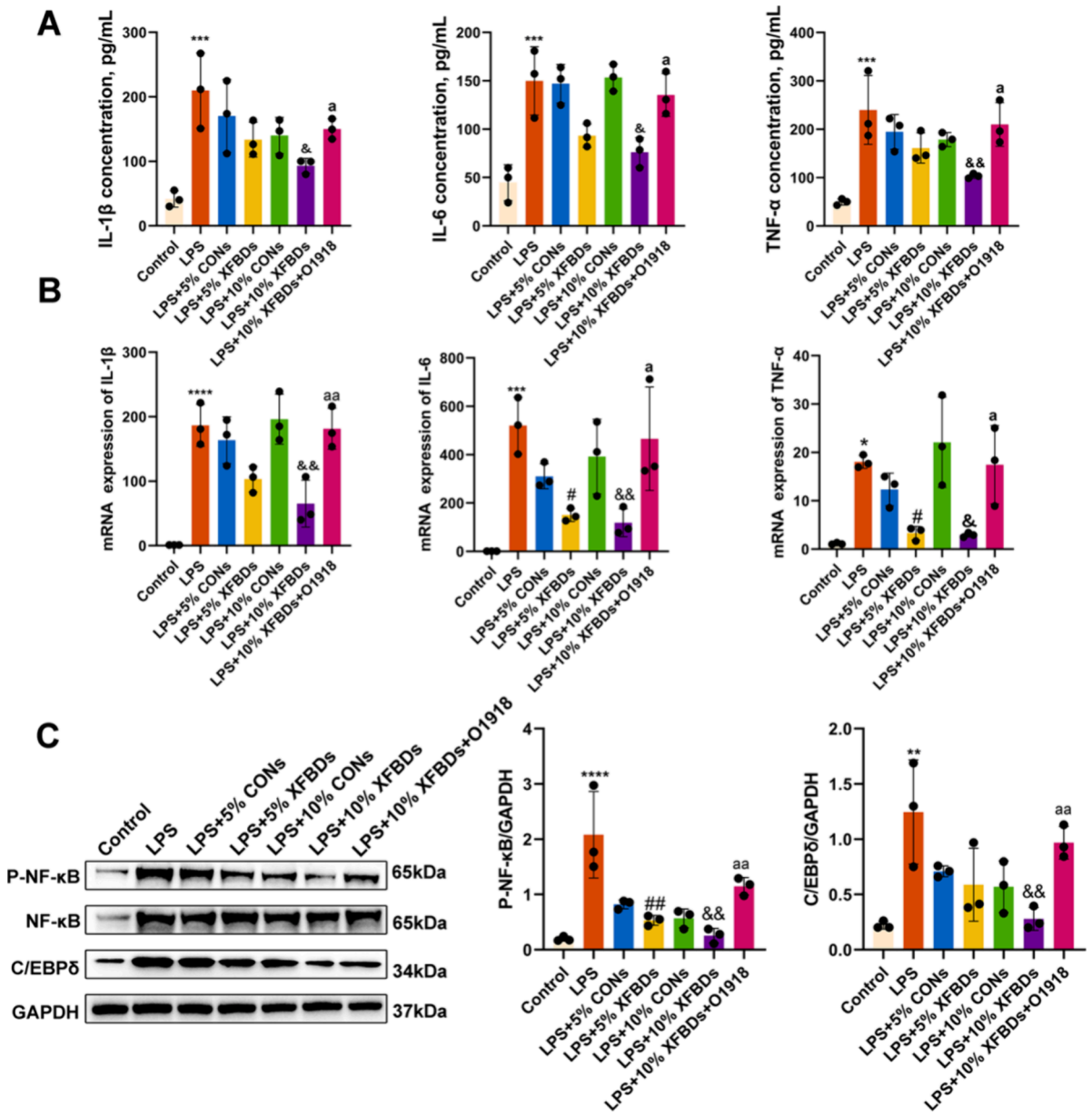

Figure 9. Effect of pretreatment with different concentrations of XFBD and GPR18 inhibitor, O1918, on an MH-S cell inflammatory model induced by LPS. (A) The effect of XFBD on the mRNA levels of inflammatory cytokines (IL-6, TNF, and IL-1β) relative to GAPDH in MH-S cells. (B) Concentrations of TNF-α, IL-1β, and IL-6 in the supernatant of LPS-stimulated MH-S cells were quantified by ELISA. (C) Protein was extracted from MH-S cells analyzed with Western blotting. XFBD may exert its anti-inflammatory effects through the NF-κB and C/EBPδ signaling pathway. Data are presented as the mean ± SEM of three independent experiments. $^{*}P < 0.05$ when compared with the Control group, $^{**}P < 0.01$ when compared with the Control group, $^{***}P < 0.001$ when compared with the Control group, $^{****}P < 0.0001$ when compared with the Control group, $^{\#}P < 0.05$ when compared with the LPS + 5% CONs group, $^{\#\#}P < 0.01$ when compared with the LPS + 5% CONs group, $^{\&}P < 0.05$ when compared with the LPS + 10% CONs group, $^{\&\&}P < 0.01$ when compared with the LPS + 10% CONs group, $^{a}P < 0.05$ when compared with the LPS + 10% XFBDs group, $^{aa}P < 0.01$ when compared with the LPS + 10% XFBDs group.

exerted anti-inflammatory effects by activating GPR18. Hence, the effects of the GPR18 inhibitor were investigated in this study. Overall, the findings demonstrated the ability of XFBD to suppress inflammatory signaling pathways and macrophage pyroptosis through GPR18 activation. Consequently, this led to a diminished release of inflammatory mediators, thus retarding ALI progression.

The findings of this study provide a material basis to support the role of XFBD in promoting inflammation resolution. Through molecular docking analysis, compounds such as 3-phenylpropyl acetate, beta-carotene, and cholesterol were identified, which are a part of XFBD and can effectively bind to GPR18. These compounds have been reported to exhibit immunomodulatory effects. For instance, in murine models, sitosterol has been shown to effectively attenuate LPS-triggered innate immune reactions, mitigating multiple organ injury and mortality.[27] The latest research shows that gastrointestinal manifestations coexist with respiratory symptoms in patients with COVID-19. COVID-19 can cause gut microbiota disorders,[28] and sepsis can also cause notable gut microbiota disorders in various cohorts of critically ill patients and animals.[29] Reportedly, XFBD can improve DSS-induced

https://doi.org/10.1021/acsomega.4c10575
ACS Omega 2025, 10, 13105−13121

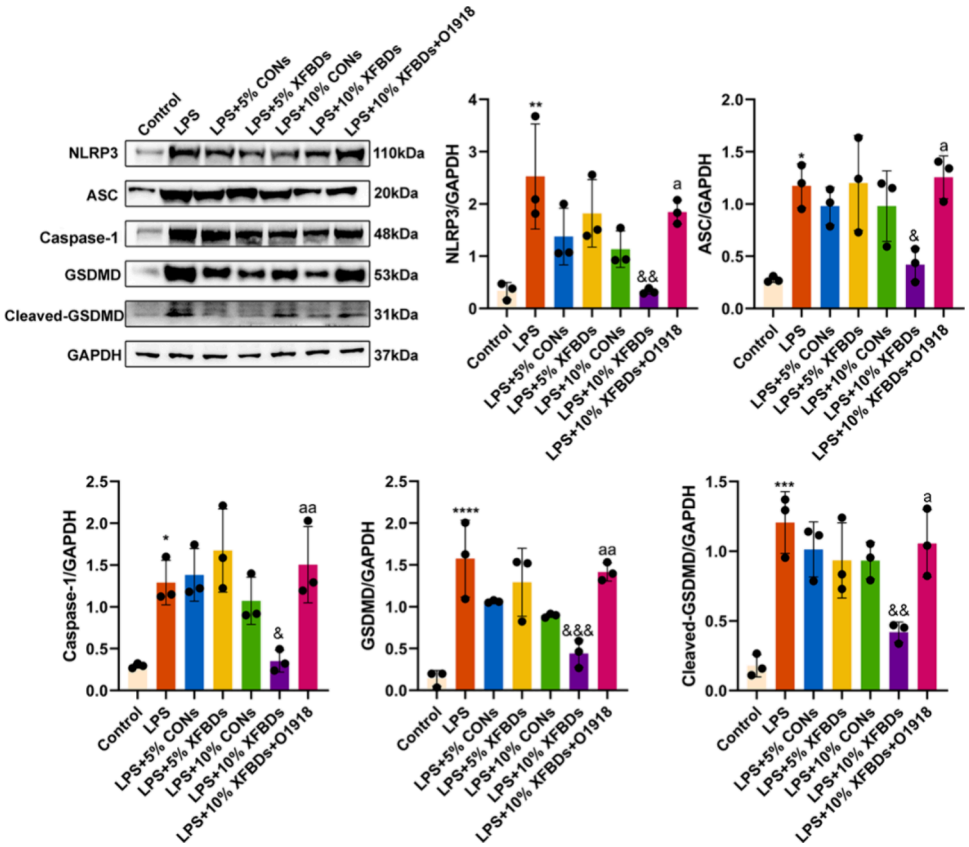

Figure 10. Effects of different concentrations of XFBD and the GPR18 inhibitor O1918 on GSDMD-mediated pyroptosis in IgG-IC-stimulated MH-S cells. Western blotting was performed to detect NLRP3, ASC, GSDMD, Cleaved-GSDMD, and Caspase-1 protein expressions. Data are presented as the mean ± SEM of three independent experiments. $^{*}P < 0.05$ when compared with the Control group, $^{**}P < 0.01$ when compared with the Control group, $^{***}P < 0.001$ when compared with the Control group, $^{****}P < 0.0001$ when compared with the Control group, $^{\&}P < 0.05$ when compared with the LPS + 10% CON group, $^{\&\&}P < 0.01$ when compared with the LPS + 10% CON group, $^{\&\&\&}P < 0.001$ when compared with the LPS + 10% CON group, $^{a}P < 0.05$ when compared with the LPS + 10% XFBD group, $^{aa}P < 0.01$ when compared with the LPS + 10% XFBDs group.

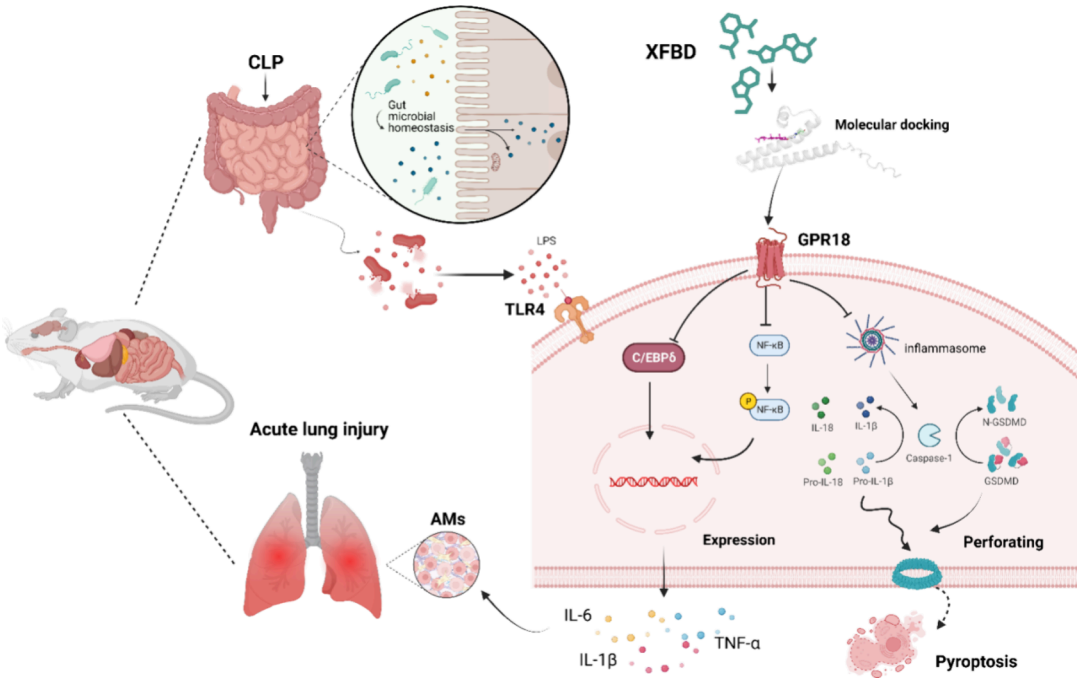

Figure 11. Schematic illustration depicting the protective effect of XFBD, which reduces the release of inflammatory factors IL-1β, IL-6, and TNF-α by activating GPR18 through the inhibition of the NF-κB and C/EBP-δ-signaling pathways while suppressing gasdermin-D-mediated pyroptosis.

https://doi.org/10.1021/acsomega.4c10575
ACS Omega 2025, 10, 13105−13121

gut microbiota disorder.[30] In the present study, we found that XFBD exhibited a notable improvement effect on the sepsis-induced microbiota disorder. Furthermore, specific alterations in microbiota composition were observed, with *Ileibacterium*, *Ileibacterium_valens*, and *Dubosiella_newyorkensis* showing increased abundance in the CLP group. Importantly, XFBD treatment markedly increased the abundance of Prevotellaceae and Ruminococcaceae_UCG_014 following CLP induction (Figure 11).

CONCLUSIONS

This study investigates the role and underlying mechanisms of XFBD in CLP-induced ALI. Along with 16S rRNA gut microbiota analysis, we elucidated XFBD-mediated amelioration of CLP-induced ALI. Altogether, the findings of this study suggest that XFBD mitigates CLP-induced ALI by restoring gut microbial equilibrium and suppressing the activation of classical pyroptosis signaling pathways, including C/EBP-δ, NF-κB, and NLRP3/Caspase-1, by activating GPR18.

AUTHOR INFORMATION

Corresponding Authors

Yuzhen Zhuo − *Tianjin Key Laboratory of Acute Abdomen Disease Associated Organ Injury and ITCWM Repair, Hospital of Integrated Chinese and Western Medicine, Tianjin University, Tianjin 300100, China;* orcid.org/0000-0002-9723-0165; Email: bluehoney1314@sina.com

Yuhong Li − *Institute of Traditional Chinese Medicine, Tianjin University of Traditional Chinese Medicine, Tianjin 301617, China;* orcid.org/0000-0002-2358-5449; Email: liyuhong@tjutcm.edu.cn

Ximo Wang − *Tianjin Key Laboratory of Acute Abdomen Disease Associated Organ Injury and ITCWM Repair, Hospital of Integrated Chinese and Western Medicine, Tianjin University, Tianjin 300100, China; Graduate School, Tianjin Medical University, Tianjin 300270, China; Tianjin Key Laboratory of Extracorporeal Life Support for Critical Diseases, Artificial Cell Engineering Technology Research Center, Tianjin Institute of Hepatobiliary Disease, Tianjin Medical University Third Center Clinical College, Tianjin 300170, China;* orcid.org/0000-0002-8070-6999; Email: wangximonkyy@126.com

Authors

Lei Yang − *Tianjin Key Laboratory of Acute Abdomen Disease Associated Organ Injury and ITCWM Repair, Hospital of Integrated Chinese and Western Medicine, Tianjin University, Tianjin 300100, China*

Sijia Zhang − *Graduate School, Tianjin Medical University, Tianjin 300270, China;* orcid.org/0000-0003-2606-6721

Lingzhi Cui − *Graduate School, Tianjin Medical University, Tianjin 300270, China*

Junxia Zhang − *Graduate School, Tianjin Medical University, Tianjin 300270, China*

Shukun Zhang − *Tianjin Key Laboratory of Acute Abdomen Disease Associated Organ Injury and ITCWM Repair, Hospital of Integrated Chinese and Western Medicine, Tianjin University, Tianjin 300100, China*

Lanqiu Zhang − *Tianjin Key Laboratory of Acute Abdomen Disease Associated Organ Injury and ITCWM Repair, Hospital of Integrated Chinese and Western Medicine, Tianjin University, Tianjin 300100, China*

Lihua Cui − *Tianjin Key Laboratory of Acute Abdomen Disease Associated Organ Injury and ITCWM Repair, Hospital of Integrated Chinese and Western Medicine, Tianjin University, Tianjin 300100, China*

Caixia Li − *Tianjin Key Laboratory of Acute Abdomen Disease Associated Organ Injury and ITCWM Repair, Hospital of Integrated Chinese and Western Medicine, Tianjin University, Tianjin 300100, China*

Complete contact information is available at: https://pubs.acs.org/10.1021/acsomega.4c10575

Author Contributions

L.Y.: Funding acquisition, Investigation, methodology, roles/writing - original draft. S.Z.: Validation; visualization; roles/writing - original draft; and writing - review and editing. L.C.: Funding acquisition, Project administration. J.Z.: Visualization, Investigation. S.Z.: Software, Validation. L.Z.: Data curation, Formal analysis, Funding acquisition. L.C.: Formal analysis; Funding acquisition C.L.: Formal analysis; Funding acquisition. Y.Z.: Visualization Y.L.: Funding acquisition, Investigation. X.W.: Funding acquisition, Investigation, Methodology, Project administration, Resources. L.Y. and S.Z. contributed equally to this article.

Notes

The authors declare no competing financial interest.
The ethical code of this project is NKYY-DWLL-2023−039.

ACKNOWLEDGMENTS

This work was financially supported by the National Key R&D Program of China (No. 2020YFA0708004), the National Natural Science Foundation of China (No. 81971858), the Inner Mongolia Natural Science Foundation (No. 2022MS08029), the Tianjin Municipal Natural Science Foundation (No. 18JCQNJC13400; No. 19JCZDJC36200), and the Science Foundation of Tianjin Municipal Health Bureau (No. 2021044).

ABBREVIATIONS

Akt:AKT serine/threonine kinase
ALI:Acute lung injury
ARDS:Acute respiratory distress syndrome
ASC:Apoptosis-associated speck-like protein
C/EBP:CCAAT/enhancer binding protein
CLP:Cecal ligation and puncture
COVID-19:Coronavirus disease 2019
ELISA:Enzyme-linked immunosorbent assay
GO:Gene Ontology
GPR18:G-protein-coupled receptor 18
GSDMD:Gasdermin D
ICAM-1:Intercellular cell adhesion molecule-1
IgG-IC:IgG immune complex
IL-17A:Interleukin-17A
IL-18:Interleukin-18
IL-1β:Interleukin-1β
IL-6:Interleukin-6
KEGG:Kyoto Encyclopedia of Genes and Genomes
LEfSe:Linear discriminant analysis effect size
LPS:Lipopolysaccharide
NF-κB:Nuclear factor kappa-B
NLRP3:NOD-like receptor protein 3

PCoA:Principal Coordinated Analysis
PD-1:Programmed cell death protein 1
RVD2:Resolvin D2
SARS-CoV-2:Severe Acute Respiratory Syndrome-Coronavirus 2
TCM:Traditional Chinese Medicine
TNF-α:Tumor necrosis factor-α
XFBD:Xuanfei Baidu Decoction

REFERENCES

(1) (a) Butt, Y.; Kurdowska, A.; Allen, T. C. Acute Lung Injury: A Clinical and Molecular Review. *Arch Pathol Lab Med.* **2016**, *140* (4), 345−350. (b) Ragaller, M.; Richter, T. Acute lung injury and acute respiratory distress syndrome. *J. Emerg Trauma Shock* **2010**, *3* (1), 43−51.

(2) Singh, G.; Gladdy, G.; Chandy, T. T.; Sen, N. Incidence and outcome of acute lung injury and acute respiratory distress syndrome in the surgical intensive care unit. *Indian J. Crit Care Med.* **2014**, *18* (10), 659−665.

(3) (a) Khilnani, G. C.; Hadda, V. Corticosteroids and ARDS: A review of treatment and prevention evidence. *Lung India* **2011**, *28* (2), 114−119. (b) Kuperminc, E.; Heming, N.; Carlos, M.; Annane, D. Corticosteroids in ARDS. *J. Clin Med.* **2023**, *12*, 3340. (c) Matuschak, G. M.; Lechner, A. J. Acute lung injury and the acute respiratory distress syndrome: pathophysiology and treatment. *Mo Med.* **2010**, *107* (4), 252−258.

(4) Varisco, B. M. The pharmacology of acute lung injury in sepsis. *Adv. Pharmacol. Sci.* **2011**, *2011*, No. 254619.

(5) (a) Cao, L.; Wang, Y.; Wang, Y.; Lv, F.; Liu, L.; Li, Z. Resolvin D2 suppresses NLRP3 inflammasome by promoting autophagy in macrophages. *Exp Ther Med.* **2021**, *22* (5), 1222. (b) Sundarasivarao, P. Y. K.; Walker, J. M.; Rodriguez, A.; Spur, B. W.; Yin, K. Resolvin D2 induces anti-microbial mechanisms in a model of infectious peritonitis and secondary lung infection. *Front Immunol* **2022**, *13*, No. 1011944. (c) Chiang, N.; de la Rosa, X.; Libreros, S.; Serhan, C. N. Novel Resolvin D2 Receptor Axis in Infectious Inflammation. *J. Immunol* **2017**, *198* (2), 842−851.

(6) (a) Zhao, M.; Zheng, Z.; Yin, Z.; Zhang, J.; Qin, J.; Wan, J.; Wang, M. Resolvin D2 and its receptor GPR18 in cardiovascular and metabolic diseases: A promising biomarker and therapeutic target. *Pharmacol. Res.* **2023**, *195*, No. 106832. (b) Fitzgerald, H.; Bonin, J. L.; Khan, S.; Eid, M.; Sadhu, S.; Rahtes, A.; Lipscomb, M.; Biswas, N.; Decker, C.; Nabage, M.; et al. Resolvin D2-G-Protein Coupled Receptor 18 Enhances Bone Marrow Function and Limits Steatosis and Hepatic Collagen Accumulation in Aging. *Am. J. Pathol.* **2023**, *193* (12), 1953−1968.

(7) Zhang, L.; Qiu, C.; Yang, L.; Zhang, Z.; Zhang, Q.; Wang, B.; Wang, X. GPR18 expression on PMNs as biomarker for outcome in patient with sepsis. *Life Sci.* **2019**, *217*, 49−56.

(8) Zhuo, Y.; Zhang, S.; Li, C.; Yang, L.; Gao, H.; Wang, X. Resolvin D1 Promotes SIRT1 Expression to Counteract the Activation of STAT3 and NF-kappaB in Mice with Septic-Associated Lung Injury. *Inflammation* **2018**, *41* (5), 1762−1771.

(9) Yang, L.; Liu, T.; Zhuo, Y.; Li, D.; Li, D.; Liu, J.; Gao, H.; Zhang, L.; Lin, J.; Wang, X. Verbenalin alleviates acute lung injury induced by sepsis and IgG immune complex through GPR18 receptor. *Cell Signal* **2023**, *109*, No. 110768.

(10) Feng, W.; Zong, W.; Wang, F.; Ju, S. Severe acute respiratory syndrome coronavirus 2 (SARS-CoV-2): a review. *Mol. Cancer* **2020**, *19* (1), 100.

(11) Liu, M.; Gao, Y.; Yuan, Y.; Yang, K.; Shi, S.; Zhang, J.; Tian, J. Efficacy and Safety of Integrated Traditional Chinese and Western Medicine for Corona Virus Disease 2019 (COVID-19): a systematic review and meta-analysis. *Pharmacol. Res.* **2020**, *158*, No. 104896.

(12) Huang, Y. F.; Bai, C.; He, F.; Xie, Y.; Zhou, H. Review on the potential action mechanisms of Chinese medicines in treating Coronavirus Disease 2019 (COVID-19). *Pharmacol. Res.* **2020**, *158*, No. 104939.

(13) Yan, H.; Lu, J.; Wang, J.; Chen, L.; Wang, Y.; Li, L.; Miao, L.; Zhang, H. Prevention of Cyclophosphamide-Induced Immunosuppression in Mice With Traditional Chinese Medicine Xuanfei Baidu Decoction. *Front Pharmacol* **2021**, *12*, No. 730567.

(14) Wang, Y.; Wang, X.; Li, Y.; Xue, Z.; Shao, R.; Li, L.; Zhu, Y.; Zhang, H.; Yang, J. Xuanfei Baidu Decoction reduces acute lung injury by regulating infiltration of neutrophils and macrophages via PD-1/IL17A pathway. *Pharmacol. Res.* **2022**, *176*, No. 106083.

(15) Xiong, W. Z.; Wang, G.; Du, J.; Ai, W. Efficacy of herbal medicine (Xuanfei Baidu decoction) combined with conventional drug in treating COVID-19:A pilot randomized clinical trial. *Integr Med. Res.* **2020**, *9* (3), No. 100489.

(16) Chu, L.; Huang, F.; Zhang, M.; Huang, B.; Wang, Y. Current status of traditional Chinese medicine for the treatment of COVID-19 in China. *Chin Med.* **2021**, *16* (1), 63.

(17) Lichota, A.; Gwozdzinski, K.; Szewczyk, E. M. Microbial Modulation of Coagulation Disorders in Venous Thromboembolism. *J. Inflamm Res.* **2020**, *13*, 387−400.

(18) (a) Shi, X.; Zhang, W.; Bao, X.; Liu, X.; Yang, M.; Yin, C. Eugenol modulates the NOD1-NF-kappaB signaling pathway via targeting NF-kappaB protein in triple-negative breast cancer cells. *Front Endocrinol (Lausanne)* **2023**, *14*, No. 1136067. (b) Wang, K.; Chen, D.; Yu, B.; He, J.; Mao, X.; Huang, Z.; Yan, H.; Wu, A.; Luo, Y.; Zheng, P.; et al. Eugenol alleviates transmissible gastroenteritis virus-induced intestinal epithelial injury by regulating NF-kappaB signaling pathway. *Front Immunol* **2022**, *13*, No. 921613. (c) Yang, L.; Li, D.; Zhuo, Y.; Zhang, S.; Wang, X.; Gao, H. Protective Role of Liriodendrin in Sepsis-Induced Acute Lung Injury. *Inflammation* **2016**, *39* (5), 1805−1813.

(19) Zhuo, Y.; Li, D.; Cui, L.; Li, C.; Zhang, S.; Zhang, Q.; Zhang, L.; Wang, X.; Yang, L. Treatment with 3,4-dihydroxyphenylethyl alcohol glycoside ameliorates sepsis-induced ALI in mice by reducing inflammation and regulating M1 polarization. *Biomed Pharmacother* **2019**, *116*, No. 109012.

(20) Yan, C.; Liu, Y.; Gao, H.; Wang, X. Suppressors of cytokine signaling 3 is essential for FcgammaR-mediated inflammatory response via enhancing CCAAT/enhancer-binding protein delta transcriptional activity in macrophages. *Exp. Cell Res.* **2015**, *337* (1), 120−127.

(21) Yan, C.; Zhang, L.; Yang, L.; Zhang, Q.; Wang, X. C/EBPgamma is a critical negative regulator of LPS-/IgG immune complex-induced acute lung injury through the downregulation of C/EBPbeta-/C/EBPdelta-dependent C/EBP transcription activation. *FASEB J.* **2020**, *34* (10), 13696−13710.

(22) (a) Zhao, L.; Liu, H.; Wang, Y.; Wang, S.; Xun, D.; Wang, Y.; Cheng, Y.; Zhang, B. Multimodal Identification by Transcriptomics and Multiscale Bioassays of Active Components in Xuanfeibaidu Formula to Suppress Macrophage-Mediated Immune Response. *Engineering (Beijing)* **2023**, *20*, 63−76. (b) Wang, Y.; Sang, X.; Shao, R.; Qin, H.; Chen, X.; Xue, Z.; Li, L.; Wang, Y.; Zhu, Y.; Chang, Y.; et al. Xuanfei Baidu Decoction protects against macrophages induced inflammation and pulmonary fibrosis via inhibiting IL-6/STAT3 signaling pathway. *J. Ethnopharmacol* **2022**, *283*, No. 114701.

(23) (a) Zhu, Y.; Luo, L.; Zhang, M.; Song, X.; Wang, P.; Zhang, H.; Zhang, J.; Liu, D. Xuanfei Baidu Formula attenuates LPS-induced acute lung injury by inhibiting the NF-kappaB signaling pathway. *J. Ethnopharmacol* **2023**, *301*, No. 115833. (b) Li, Z.; Pan, H.; Yang, J.; Chen, D.; Wang, Y.; Zhang, H.; Cheng, Y. Xuanfei Baidu formula alleviates impaired mitochondrial dynamics and activated NLRP3 inflammasome by repressing NF-kappaB and MAPK pathways in LPS-induced ALI and inflammation models. *Phytomedicine* **2023**, *108*, No. 154545. (c) Li, C.; Li, Y.; Zhang, H.; Zhuo, Y.; Zhang, L.; Yang, L.; Gao, Q.; Tu, Z.; Shao, R.; Wang, Y.; et al. Xuanfei Baidu Decoction suppresses complement overactivation and ameliorates IgG immune complex-induced acute lung injury by inhibiting JAK2/STAT3/SOCS3 and NF-kappaB signaling pathway. *Phytomedicine* **2023**, *109*, No. 154551.

(24) Pritts, T.; Hungness, E.; Wang, Q.; Robb, B.; Hershko, D.; Hasselgren, P. O. Mucosal and enterocyte IL-6 production during

https://doi.org/10.1021/acsomega.4c10575
ACS Omega 2025, 10, 13105−13121

sepsis and endotoxemia–role of transcription factors and regulation by the stress response. *Am. J. Surg* **2002**, *183* (4), 372−383.
(25) (a) Zheng, X.; Chen, W.; Gong, F.; Chen, Y.; Chen, E. The Role and Mechanism of Pyroptosis and Potential Therapeutic Targets in Sepsis: A Review. *Front Immunol* **2021**, *12*, No. 711939. (b) Gao, Y. L.; Zhai, J. H.; Chai, Y. F. Recent Advances in the Molecular Mechanisms Underlying Pyroptosis in Sepsis. *Mediators Inflamm* **2018**, *2018*, No. 5823823.
(26) Sun, X.; Liu, Y.; Huang, Z.; Xu, W.; Hu, W.; Yi, L.; Liu, Z.; Chan, H.; Zeng, J.; Liu, X.; et al. SARS-CoV-2 non-structural protein 6 triggers NLRP3-dependent pyroptosis by targeting ATP6AP1. *Cell Death Differ.* **2022**, *29* (6), 1240−1254.
(27) Antwi, A. O.; Obiri, D. D.; Osafo, N.; Forkuo, A. D.; Essel, L. B. Stigmasterol inhibits lipopolysaccharide-induced innate immune responses in murine models. *Int. Immunopharmacol* **2017**, *53*, 105−113.
(28) Dhar, D.; Mohanty, A. Gut microbiota and Covid-19- possible link and implications. *Virus Res.* **2020**, *285*, No. 198018.
(29) Adelman, M. W.; Woodworth, M. H.; Langelier, C.; Busch, L. M.; Kempker, J. A.; Kraft, C. S.; Martin, G. S. The gut microbiome's role in the development, maintenance, and outcomes of sepsis. *Crit Care* **2020**, *24* (1), 278.
(30) Ma, L.; Zhao, X.; Liu, T.; Wang, Y.; Wang, J.; Kong, L.; Zhao, Q.; Chen, Y.; Chen, L.; Zhang, H. Xuanfei Baidu decoction attenuates intestinal disorders by modulating NF-kappaB pathway, regulating T cell immunity and improving intestinal flora. *Phytomedicine* **2022**, *101*, No. 154100.

https://doi.org/10.1021/acsomega.4c10575
ACS Omega 2025, 10, 13105−13121